Article:
Alzaza, A., Ohenoja, K., Isteri, V. et al. (4 more authors) (2022) Blending eco-efficient calcium sulfoaluminate belite ferrite cement to enhance the physico–mechanical properties of Portland cement paste cured in refrigerated and natural winter conditions. Cement and Concrete Composites, 129. 104469. ISSN 0958-9465

https://doi.org/10.1016/j.cemconcomp.2022.104469

Cement and Concrete Composites 129 (2022) 104469

Contents lists available at ScienceDirect

Cement and Concrete Composites

journal homepage: www.elsevier.com/locate/cemconcomp

Blending eco-efficient calcium sulfoaluminate belite ferrite cement to enhance the physico–mechanical properties of Portland cement paste cured in refrigerated and natural winter conditions

Ahmad Alzaza [a,*], Katja Ohenoja [a], Visa Isteri [b], Theodore Hanein [c], Daniel Geddes [c], Minna Poikelispää [d], Mirja Illikainen [a]

[a] Fiber and Particle Engineering Research Unit, Faculty of Technology, University of Oulu, P.O. Box 4300, 90014, Oulu, Finland
[b] Process Metallurgy, Faculty of Technology, PO Box 4300, 90014, University of Oulu, Finland
[c] Department of Materials Science and Engineering, The University of Sheffield, Sheffield, S1 3JD, UK
[d] Tampere University, Faculty of Engineering and Natural Sciences, P.O. Box 589, FI-33014, Tampere, Finland

ARTICLE INFO

Keywords:
Cold weather concreting
Refrigerated curing
Freezing point
Compressive strength
CSA cement
Belite ye'elimite ferrite

ABSTRACT

The acceleration impacts of calcium sulfoaluminate belite ferrite (CSABF)—a cement produced from industrial side streams—on the hydration and strength development of Portland cement (PC) paste cured at −5 °C with and without pre-curing at room temperature were investigated. The impacts of eco-friendly CSABF cement content and pre-curing on the setting time and hardened properties of pastes were investigated. Freezing point of the paste and the amount of freezable water (FW) decreased with CSABF cement content and pre-curing. Hydration rate increased with CSABF cement content. By adding an optimal CSABF cement content, the compressive strength of paste cured at −5 °C increased by 500%. The effects of pre-curing on the compressive strength of the subzero-cured pastes were highly dependent on CSABF cement content and curing period. After 6 months, the outdoor-cured 70%PC/30%CSABF paste gained compressive strength comparable to that in the 90-day-old pair cured at −5 °C and continuous strength gain was detected up to one-year. The microstructural observations and porosity results are consistent with compressive strength measurements.

1. Introduction

Harsh cold weather conditions and long winter season are among the main challenges for the construction sector in northern regions. When the ambient temperature drops below the optimal curing temperature (i.e., 10 °C-20 °C), the setting time and strength development rate of Portland cement (PC)-based concrete are decelerated due to the diminished reaction rate between cement and water [1–3]. The slow setting time and strength development not only prolong the construction period but also increase the collapse risk of weak structures. In addition, the hydration process of PC ceases when the ambient temperature drops below the freezing point of concrete pore solution, as ice crystals start to form, and thus the liquid-state water will no longer be available for the subsequent hydration process. Furthermore, the early freezing of concrete can lead to a 50% reduction in compressive strength and frost resistance as a result of the microstructural damage and crack propagation induced by the expanded volume (≈9%) of nucleated ice crystals and increased internal stress [4]. At present, technologies, such as heating systems, heated raw materials, insulation blankets, ultra-fine and rapid hardening cement, antifreeze admixtures, and so on, are employed to avoid early freezing risk in concrete and accelerate its strength development under cold weather conditions [1,5]. However, these means increase the complexity, cost, and energy consumption of cold-weather construction works [2]. Thus, winter construction activities are usually avoided in northern regions, which shortens their construction season and impedes their urban and infrastructure developments.

Currently, cost-efficient and environmentally friendly binders that can harden at low ambient temperatures (<5 °C) are needed, along with decreased demand for energy-intensive and costly heating systems, to reduce the cost and environmental load of cold-weather concreting activities. Calcium sulfoaluminate (CSA) cement is known for its faster hydration rate, setting time, and strength development when compared with PC, therefore it has been used as eco-cement for cold weather concreting works [1,2,6,7]. These advantages of CSA accompanied with its lower associated carbon footprint than PC [8,9], make it suitable for cold weather

* Corresponding author.
E-mail address: Ahmad.Alzaza@oulu.fi (A. Alzaza).

https://doi.org/10.1016/j.cemconcomp.2022.104469
Received 10 November 2021; Received in revised form 2 February 2022; Accepted 1 March 2022
Available online 12 March 2022

construction works, especially where quick re-use, such as roads and airport runways, is required. Typically, the main components in CSA cement include 30–70 wt% ye'elimite ($C_4A_3\$$), 10%–25% calcium sulfate (gypsum [$C\$H_2$] or anhydrite [$C\$$]), mayenite ($C_{12}A_7$), and belite (C_2S) [10]. The main reaction products of CSA cement with gypsum are ettringite (AFt) and amorphous aluminum hydroxide (AH_3) [11,12]. Once the available soluble calcium sulfate has been exhausted, ye'elimite can continue to hydrate to form a monosulfoaluminate (AFm) and additional AH_3 [13]. Furthermore, Telesca et al. [14] and Wolf et al. [15] reported that when the sulfate content in the PC/CSA blend is sufficient, it can achieve a faster hardening rate compared with pure CSA cement-based binder, which is preferable in cold weather concreting works. Recently, the use of CSA cement at subzero temperatures has been investigated by different researchers, either as a sole binder or as a mineral accelerator in PC/CSA blends, showing great potential for use in cold weather concreting works [1,2,6,7]. Huang et al. [1] assessed the reactivity and strength development of a binder consisting of commercially available CSA cements at subzero curing temperatures (i.e., −5 °C and −10 °C), showing faster early hydration and strength development of CSA cement binder compared with that in PC-based binder. However, the 28-day compressive strength of the CSA-based mortar (w/c = 0.5) cured at −5 °C decreased by 65% compared with that cured at 20 °C [1]. Similarly, when the binders were cured initially at −5 °C before being exposed to standard curing conditions (i.e., 20 °C), Li et al. [2] and Qin et al. [6] reported faster reactivity and strength development, as well as better early age frost resistance in PC/CSA blends, compared with those measured in PC binder. Moreover, Zhang et al. [7] used commercially available CSA cements as a mineral accelerator for PC paste cured at −5 °C and reported a significant increase in the 28 d compressive strength (~300%), with no risk of freezing when an optimal amount of CSA was added. They attributed the enhanced subzero performance of CSA cement-containing binders to the rapid precipitation of AFt and accelerated setting time.

The higher cost of commercially available CSA cement compared with that of PC has limited the widespread use of CSA cement as a potential eco-friendly alternative/additive [16]. The availability of alumina-rich raw materials for manufacturing has locational limitations that affect the sustainability and supply of CSA cement [17]. Nevertheless, such limits (i.e., costs and availability of raw materials) can be overcome by manufacturing belite CSA ferrite (CSABF) clinker with low ye'elimite content and high belite and ferrite proportions [11]. Recently, different industrial side streams, such as fly ash, dealkalized red mud, aluminum ash, carbide slag, flue gas desulfurization, gypsum, ladle slag, iron-slag, phosphogypsum, and so on, have been utilized in the production of eco-BCSA/CSABF cement [11,18–21]. Scale-up production of CSABF clinkers produced from ladle slag, iron-slag, and phosphogypsum has recently been demonstrated and reported by Isteri et al. [17]. The utilization of industrial side streams instead of virgin materials can decrease the cost of these special types of cement and increase the potential of local production and their wide-scale use without affecting the costs of construction projects.

This experimental work investigates the potential acceleration influence of an eco-efficient CSABF cement manufactured utilizing industrial residues (i.e., ladle slag, iron-slag, and phosphogypsum) [17] on the reactivity and strength gain of PC-based paste cured at −5 °C and natural Finnish winter conditions. PC was blended with varied amounts of CSABF cement (i.e., 10–40 wt%). In addition, the effects of the 2 h pre-curing period at room temperature (22 ± 1 °C) were assessed. The freezing point of paste and the amount of freezable water (FW) were measured by low-temperature differential scanning calorimetry (LT-DSC). Reactivity and hydration products of pastes were investigated by isothermal calorimetry, setting time, quantitative X-ray diffraction (XRD), and thermogravimetric/differential thermogravimetry (TGA/DTG) analyses. Scanning electron microscopy (SEM) was used for the microstructural assessments, and porosity was measured by mercury intrusion porosimetry (MIP). The mechanical properties were evaluated in terms of compressive strength.

2. Experimental

2.1. Materials

PC (CEM I 52.5R) was supplied by Finnsementti (Finland), and eco-efficient CSABF clinkers produced by Isteri et al. [17] were used. A synthetic gypsum (VWR, Germany) was employed as a calcium sulfate source in a mixture of CSABF clinkers and gypsum at a mass ratio of 4:1, resulting in sulfate/ye'elimite molar ratio (M-value) equal to 2.27. The particle size distribution of the PC, CSABF clinkers, and gypsum were measured in isopropanol using a particle size analyzer (LS 13320 from Beckman Coulter, USA) and shown in Fig. 1. The median particle size was 8, 7, and 10 μm for PC, CSABF clinkers, and gypsum, respectively. The chemical compositions of the used materials were assessed by X-ray fluorescence using a PANalytical Omnian Axiosmax at 4 kV, and the main mineralogical phases were measured by quantitative XRD (Q-XRD) (additional details are shown in Section 2.3.5; Table 1). XRD patterns of PC and CSABF clinker are shown in Appendix A (see Fig. A1). Detailed production procedures, chemical and physical properties, and impurity contents of the CSABF clinkers can be found elsewhere [17]. A polycarboxylate-based superplasticizer (SP, Sika® Viscocrete-5800) with a solid content of approximately 35.5% was used. Petkova et al. [22] reported that this superplasticizer has no retarding effects on hydration kinetics. Deionized water was used in the preparation of pastes. All raw materials were stored at lab conditions (22 ± 1 °C) before use.

2.2. Paste sample preparation and curing conditions

PC/CSABF blend mix proportions/designs are shown in Table 2. Five binders were developed in this study to assess the impacts of replacing PC with eco-CSABF cement on the mineralogy, reactivity, and strength development of PC/CSABF binders cured at −5 °C. To prepare PC/CSABF binders, we replaced PC with 10, 20, 30, and 40 wt% CSABF cement. For comparison purposes, a reference binder (C0) consisting of 100% PC was prepared. For all binders, the water-to-cement (PC or PC + CSABF cement) ratio (w/c) was kept constant at 0.27, considering the water content in SP [23]. The dosage of SP was adjusted (through preliminary experiments) and varied between 0.5% and 1.5% by the total mass of the cement (PC or PC + CSABF cement); this value is within the company recommended dosage (0.5–2 wt.%).

For mixing, first, the dry raw materials (i.e., PC, CSABF clinker, and gypsum) were mixed using the Hobart mixer for at least 30 min to achieve good homogeneity. SP was added to the mixing deionized water and maintained in an ultrasonic bath (Elmasonic P, Germany) for 5 min [23]. Thereafter, the deionized water, including SP, was added to the mixed dry ingredients and mixed thoroughly for 3 min at lab-controlled

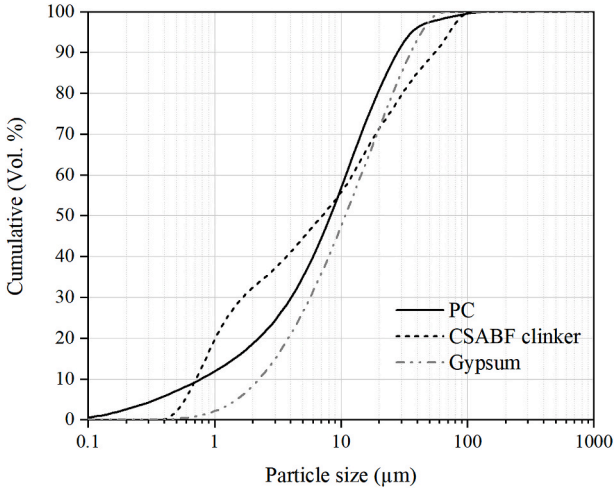

Fig. 1. Particle size distribution of the raw materials.

Table 1
Chemical composition and mineralogy (wt.%) of the raw materials.

XRF				Q-XRD			
Oxide	PC	CSABF clinker	Gypsum	Phase	PC	CSABF clinker	Gypsum
CaO	69.0	46.8	32.3	C_3S	61.0	–	–
SiO_2	24.0	13.8	0.7	C_2S	25.3	28.9	–
Al_2O_3	2.1	23.1	0.1	C_3A	4.2	5.3	–
Fe_2O_3	0.3	10.7	0.1	Bassanite; hemihydrate	1.5	–	–
MgO	0.7	4.8	0.4	C$ ·2H	3.4	–	98.2
SO_3	2.3	5.8	42	$C_4A_3$$	–	31.3	–
Na_2O	-	0.3	-	C_2(A,F)	–	8.7	–
K_2O	-	0.1	-	$C_{12}A_7$	2.0	2.0	–
TiO_2	-	0.8	-	M	0.1	4.4	–
LOI (950 °C)	0.8	0	21.3	S	0.4	1.4	–
				C_2AS	–	6.1	–
				C $	–	1.7	1.7
				C_3T(F,A)	–	0.6	–
				F	–	1.1	–
				$CaMg(CO_3)_2$	1	–	–
				Lime	1	–	
				Portlandite	1.2	–	–
				Amorphous	0	2.7	–

M: Periclase; S: Quartz; and F: iron Fe_2O_3.

Table 2
Mix proportions (by mass) of prepared pastes.

Sample ID	PC (g)	CSABF cement (g)	SP (g)	w/c
C0	100	0	0.5	
C10	90	10	0.6	
C20	80	20	0.75	0.27
C30	70	30	1	
C40	60	40	1.5	

conditions (22 ± 1 °C). The fresh pastes were then cast into prismatic molds (20 mm × 20 mm × 80 mm), compacted using a jolting table (120 shocks, 1 shock/s), and sealed with a plastic bag to avoid moisture loss [24]. The pastes in the molds were then cured in a pre-set freezer at −5 °C, with and without the 2 h pre-curing period at 22 ± 1 °C. Moreover, the best performing paste mix composition (in terms of early compressive strength development) was selected to assess the impacts of natural Finnish winter conditions (with and without the 2 h pre-curing period at room temperature) on the strength development. The average air temperature during the outdoor curing period (17th Dec. 2020 – 21st Jun. 2021 in Oulu, Finland, 65°01′ N, 25°28′ E) is shown in Appendix A (see Fig. A2). During this period, the ambient temperature fluctuated between −23 °C and 19 °C. To simulate construction site conditions, we kept the molds for the freezer- and external-cured samples without the 2 h pre-curing in the freezer (−5 °C) and external conditions for 24 h before casting, respectively; molds for samples pre-cured for 2 h were kept at room temperature [25].

2.3. Test methods

2.3.1. Heat of hydration

An isothermal calorimeter (Thermometrics TAM air) was used at 23 °C to monitor the impacts of CSABF content on the very early dissolution rate, as well as the heat evolution and reaction rate during the pre-curing period. Given the difficulty of in-situ mixing with w/c of 0.27 due to the limited rotation speed of the InMixEr tool, the mixing procedures were carried out as follows:

- For in-situ mixing (to monitor the dissolution peak): 2 g of dry cement (PC or PC + CSABF cement) were filled in a glass ampule, and 1 g of water (w/c = 0.5) was sucked into the InMixer syringe. Thereafter, the InMixer with the filled materials was placed in the instrument and equilibrated at 23 °C for 24 h. The water was then injected into dry ingredients, and both were mixed inside the instrument.
- For ex-situ mixing (to follow the hydration rate): pastes were prepared according to the procedure listed in Section 2.2 (w/c = 0.27). Approximately 5 g of paste was then poured into the glass ampules and loaded into the isothermal calorimeter immediately.

In both cases, water was used as a reference sample, and the measured heat flow and calculated cumulative released heat were normalized by the weight of the paste.

2.3.2. Setting time

The setting times of paste samples were determined using an automated Vicat apparatus (Matest E044 N, Italy) at 22 ± 1 °C according to EN196-3 standard [26]. The initial and final setting times were reported when the distance from the needle to the bottom was 6 ± 3 mm and 39.5 mm while using a cylindrical mold (inner diameter of 80 mm and height of 40 mm), respectively.

2.3.3. Determination of freezing point and amount of freezable water

The effects of CSABF cement content and pre-curing on the freezing point and amount of free freezable water of the binders were investigated using the LT-DSC (NETZSCH DSC 214). Samples were prepared according to the procedure listed in Section 2.2, and approximately 40–50 mg of samples (exact weights recorded) were poured into an aluminum crucible. For the paste without the 2 h pre-curing period, the crucible was placed immediately in the machine, and the test was performed with the following temperature program: at −30 °C for 5 min and then raised from −30 °C to 25 °C at a rate of 5 °C/min (see Fig. 2 [a]) [7]. For the paste with the 2 h pre-curing period, the crucible was sealed with an aluminum lid at room temperature (22 ± 1 °C) for 2 h and then tested following the above-mentioned procedures. In cementitious materials, the only phase change that occurs within the temperature range of −30 °C–25 °C is related to the pore solution [27]. The endothermic peak (Fig. 2 [b]) represents the melting signal of the frozen pore solution. The intersection point of the tangent line and baseline of the initial melting curve is the melting point of the frozen pore solution (i.e., freezing point) [27]. Thereafter, Eq. (1) was used to estimate the percentage of FW using the integral area of the melting peak (Fig. 2 [c]) [28,29].

$$\text{FW}\ \ (\%) = \left(\frac{Q}{H_f \times m}\right) \times 100 \quad (1)$$

where Q is the enthalpy (J), H_f is the heat of fusion of water (333.5 J/g), and m refers to the mass of the sample (g).

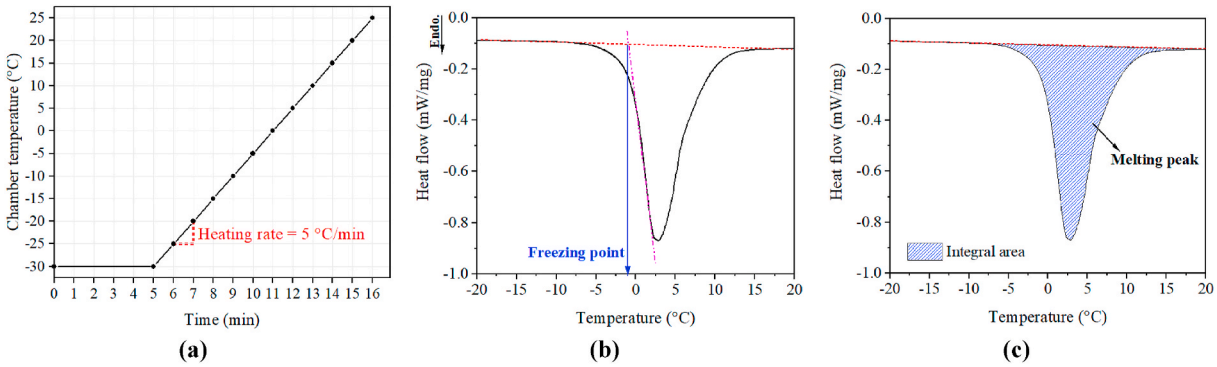

Fig. 2. (a) Temperature program for freezing–thawing cycle in LT-DSC, (b) freezing point determination method, and (c) melting heat (i.e., amount of frozen water) determination.

2.3.4. Compressive strength

The compression test was performed using 20 mm cubes. A calibrated Zwick/Roell (Z400) compressive test machine with a load cell of 100 kN was used. The average and standard deviation of six cubes were reported for each data point. The samples were stored for approximately 30–40 min at room temperature before testing to eliminate the potential impacts of any formed ice in the pore structure on compressive strength measurements [30].

2.3.5. Hydration product evolution

The hydration products were assessed by XRD and TGA/DTG analyses. At the designated age, hydration was stopped by the solvent exchange technique using isopropanol, and the solution was changed twice during the first 2 h and then kept for 48 h. The soaking time in isopropanol was determined according to the Zhang and Scherer [31] diffusion model, using samples size ranging between 1.5 and 2 mm and isopropanol diffusion coefficient of 3×10^{-12} m^2/s. Thereafter the samples were removed from isopropanol and dried in a desiccator at room temperature until the analysis date. Samples were crushed and powdered for XRD and TGA/DTG analyses. XRD data were collected using a Rigaku SmartLab 9 kW diffractometer. A CoKα radiation at 40 kV and 135 mA, a step size of 0.02°, and a scanning rate of 4°2Θ/min were employed over a 2Θ range of 5°–130°. Phase identification was conducted using Rigaku PDXL 2 software with PDF-4+ 2020 RDB database, and whole powder pattern fit analysis using the Rietveld method was employed to calculate the quantities of the main phases in the samples. The R_{wp} values of the analyses were between 3% and 5%. Internal standard TiO_2 (20 wt%) was used to estimate the trend of amorphous content in the hydrated samples. TGA/DTG data were collected using an SDT-650 Thermal analyzer (TA® instruments, USA). The powder specimens (≈15 mg each) were heated from 25 °C to 500 °C at 10 °C/min in an inert nitrogen atmosphere.

2.3.6. Morphology and porosity assessment

The morphology of selected pastes was assessed using field emission SEM (Zeiss ULTRA plus FESEM, Germany). The samples were extracted from the core of untested pastes and the hydration was stopped according to the procedures mentioned in Section 2.3.5. Thereafter, the samples were mounted in epoxy resin and then polished with diamond pastes. The analysis was carried out using carbon-coated specimens under a backscatter electron (BSE) detector at an acceleration voltage of 15 kV. The porosities of hardened paste samples were characterized by MIP using a Micromeritics Autopore V. The samples were extracted from the core of intact samples and were pre-dried and weighed 1.0 ± 0.2 g. The pressure was gradually reduced to 50 μmHg; mercury with a surface tension of 0.485 Nm^{-1} was filled; and the intrusion was measured to 60,000 PSI. A contact angle of 130° was used for these measurements [32].

3. Results and discussion

3.1. Heat of hydration

In the cement hydration process, the initial exothermic peak (0 min–30 min), which is also known as the dissolution peak, is mainly attributed to the cement wetting, ion dissolution, and initial precipitation of AFt [7,33–35]. Fig. 3 (in-situ; w/c = 0.5) shows that the height of the dissolution peak was enhanced with the addition and content of CSABF cement, indicating the accelerated release of ions. The improved intensities of dissolution peaks of the PC/CSABF binder can be attributed to the increased amount of total available sulfate, rapid dissolution of the ye'elimite ($C_4A_3\$$), tricalcium aluminate (C_3A), and mayenite ($C_{12}A_7$) phases from CSABF clinker, and accelerated precipitation of early-formed AFt due to fast reaction rate between $C_4A_3\$$, C_3A,and $C_{12}A_7$ with gypsum (Eq. [2–4]) [15,34,36,37]. As a result, the C0 showed a dissolution peak with no more than 13 mW/g, whereas 15, 23, 29, and 32 mW/g were measured in C10, C20, C30, and C40, respectively.

In the ex-situ pastes (w/c = 0.27), the CSABF cement accelerated the appearance of the acceleration peak (i.e., increased hydration rate) at 23 °C, especially when the replacement level was higher than 10% (Fig. 4 [a]). The acceleration peak was observed for approximately 9 h (7.9 mW/g) in C0. This peak in PC hydration corresponds to the rapid dissolution of C_3S and rapid precipitation of CH and C–S–H phases [7]. The acceleration peaks of PC/CSABF binders were found earlier (i.e., shorter induction period), narrower, and higher in amount compared with that of C0. When PC was replaced with only 10 wt% CSABF cement, the induction period was slightly shortened, and the acceleration peak

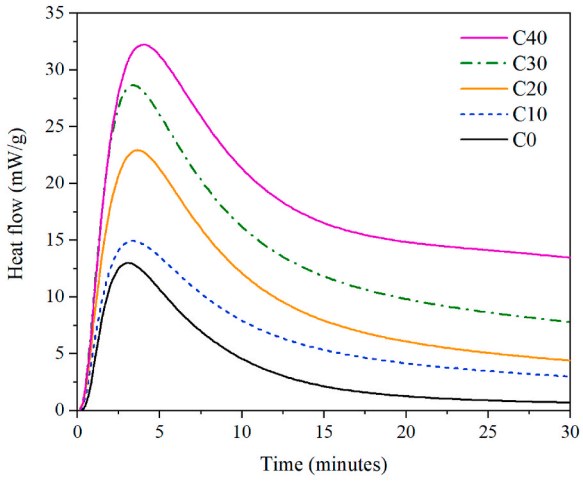

Fig. 3. Impacts of CSABF cement content on the dissolution peak and early ettringite precipitation of in situ mixed pastes (w/c = 0.5) at 23 °C.

was observed at approximately 6.7 h (8.4 mW/g). Once the replacement level was ≥20%, the appearance of the acceleration peaks was significantly accelerated and detected at approximately 2.3 h (11.9 mW/g), 0.6 h (18.4 mW/g), and 0.25 h (47.1 mW/g) in C20, C30, and C40, respectively. The accelerated appearance and higher acceleration peak intensities in the PC/CSABF binders are mainly attributed to the faster and more intensive precipitation of AFt [38]. Moreover, the eco-CSABF clinker contains 5.3 wt% of C_3A and 2 wt% of mayenite ($C_{12}A_7$) (see Table 1), which accelerates the early hydration process of PC-based systems by accelerating the consumption of gypsum and the formation of an additional AFt phase [33].

$$C_4A_3\$ + 2\ C\$H_2 + 34\ H \rightarrow C_6A\$_3H_{32} + 2\ AH_3 \quad (2)$$

$$C_3A + 3\ C\$H_2 + 26\ H \rightarrow C_6A\$_3H_{32} \quad (3)$$

$$C_{12}A_7 + 12C\$H_2 + 137\ H \rightarrow 4\ C_6A\$_3H_{32} + 3\ AH_3 \quad (4)$$

The cumulative released heats of hydration during the first 2 h of the measurement period, representing the pre-curing period, are displayed in Fig. 4 (b). The released heat during the first 2 h was increased considerably with the addition and content of CSABF cement. The order of cumulative released heat after 2 h was C30 (13.1 J/g) > C20 (9.9 J/g) > C40 (9.4 J/g) > C10 (5.4 J/g) > C0 (1.2 J/g). The higher released heats during the first 2 h from the PC/CSABF compared with that from C0 indicate greater hydration progress and reaction products precipitation in the presence of CSABF cement during the pre-curing period. The heat of hydration measurements are in line with reaction product evolution (as shown later in Section 3.5). Taylor [39] reported that the cumulative heat of hydration indicates the hydration degree of the binders and the amount of precipitated reaction products. Interestingly, the C40 binder showed a lower 2 h cumulative released heat than C20 and C30; this result can be attributed to the early formation of impermeable (or semi-impermeable) rim around the anhydrous PC and CSABF cement particles due to the rapid early precipitation of AFt and aluminium hydroxide in the C40 binder. This rim densifies the paste microstructure and hinders water diffusion into anhydrous cement particles, hence suppressing the subsequent dissolution process and deaccelerating the follow-up hydration reaction [2,33,40].

3.2. Setting time

In line with the heat of hydration observations, replacing PC with CSABF significantly accelerated the initial and final setting times (22 ± 1 °C) of the pastes (Fig. 5). The initial (220 min) and final (270 min) setting times of the C0 were decreased to 15 min and 20 min in the C40 binder, indicating the rapid early hydration and precipitation of reaction products in the blended binders, respectively. Moreover, the period between the initial and final setting times was also shortened with the incorporation of CSABF cement. The accelerated setting times of PC/CSABF binders are mainly associated with the fast hydration rate of $C_4A_3\$$ in the presence of gypsum. The latter results in the rapid precipitation of overlapping needle-like AFt, forming an interconnected AFt network that consumes a large amount of mixing water (Eq. [2]) and dispersed residual mixing water into irregular micron-sized pores within the AFt skeleton [2,6,35,38]. As a result, PC/CSABF pastes underwent a rapid loss of plasticity and rapid hardening, which illustrates the accelerated setting times even with low CSABF cement dosage (i.e., 10%). Notably, accelerated setting times are preferable in low-temperature construction activities, especially for winter infrastructure and traffic maintenance works where rapid turnaround is required. However, the short setting times are challenging, and thus well-prepared casting areas and the availability of experienced workers should be assured before mixing to insure finalizing the casting before the setting times. Alternatively, a retarder (e.g., citric acid [41]) can extend the setting time of the blends, thus broadening the application range of these materials.

3.3. Freezing point and freezable water

The freezing points of the binder pore solutions were depressed using CSABF cement content and the 2 h pre-curing period (Table 3 and

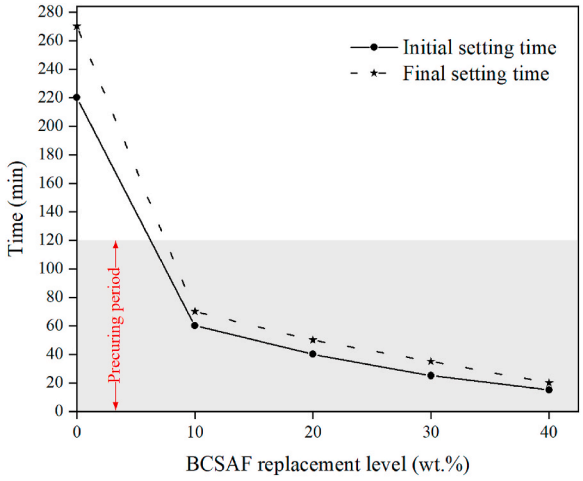

Fig. 5. Impacts of CSABF content on setting time of binders measured at room temperature.

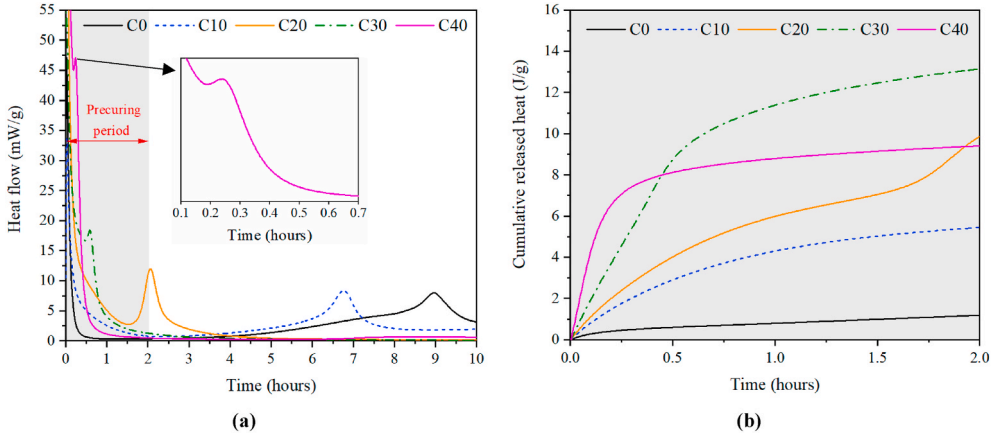

Fig. 4. (a) Heat flow and (b) cumulative heat of hydration of ex-situ mixed pastes (w/c = 0.27) at 23 °C. The cumulative released heat was calculated by the integration of measured heat flow after 10 min of ampoules inserting time into calorimeter slot to exclude the peak caused by the chamber's environment disturbance.

Fig. A3). The freezing point of the control binder without pre-curing [C0-(0 h)] was approximately −1.3 °C. This finding shows that the liquid phase (i.e., pore solution) of C0 will freeze when subjected to the curing temperature of this study at −5 °C. When PC was replaced with CSABF cement, the freezing points of the C10-(0 h), C20-(0 h), C30-(0 h), and C40-(0 h) binders were depressed to −2.9 °C, −3.5 °C, −5.3 °C, and −5.5 °C, respectively. The latter indicates that replacing PC with CSABF cement can protect the binders against freezing at a −5 °C curing temperature when the replacement level is ≥ 30%. The lower freezing points of CSABF-containing binders (without pre-curing) compared with that of PC-binder (C0-[0 h]) can be attributed to the higher early ion concentration in the pore solution due to the faster ion dissolution and hydration rates, as shown in Fig. 3 in Section 3.1 [7,42,43].

The freezing points of the binders were further decreased with the 2 h pre-curing period. The impacts of the pre-curing on the freezing point depression extent were more evident in the PC/CSABF binders compared that in the C0. Therefore, the freezing point of C0-(2 h) was negligibly depressed with the pre-curing to approximately −1.4 °C due to its limited hydration progress during the first 2 h of the curing period (see Fig. 4 [b]). This result shows that the short pre-curing period was unable to protect the C0 against freezing at −5 °C curing temperature (compressive strength results in Section 3.4.1 confirm this observation). Due to the 2 h pre-curing period, the freezing points of C10-(2 h), C20-(2 h), C30-(2 h), and C40-(2 h) were considerably depressed to approximately −4.1 °C, −5.7 °C, −6.2 °C, and −6.7 °C, respectively. As shown earlier (Section 3.1), the addition of CSABF cement significantly accelerated early dissolution (Fig. 3) and enhanced the hydration degree (Fig. 4 [b]). This method increases the ion concentration in the pore solution, consumes a considerable amount of free water, and decreases the pore size. The freezing point of the pore solution in porous materials is depressed with increased ion concentration "concentration effect" [42,43] and decreased pore radius "network effect" [44–48]; therefore, the additional depression in the freezing points of the PC/CSABF binders after the 2 h pre-curing period may be attributed to the mutual impacts of concentration and network effects.

In addition, increasing the CSABF cement content and the 2 h pre-curing period decreased the melting heat (i.e., amount of FW), indicating the accelerated consumption of free water (Fig. 6). Regarding the results, C0-(0 h) exhibited the highest amount of FW, whereas a 3.7%, 17.6%, 22.5%, and 24.4% decrease in the amounts of FW were calculated in the C10-(0 h), C20-(0 h), C30-(0 h), and C40-(0 h) compared with that of C0-(0 h), respectively. Promisingly, the impacts of the 2 h pre-curing period on the amount of FW were significant in the CSABF cement-containing binders. Therefore, only an 8.2% decrease in the amount of FW was calculated in C0-(2 h) compared with that in C0-(0 h). By contrast, approximately 17.8%, 23.2%, 36.1%, and 34.9% reductions in the amounts of FW were reported in C10-(2 h), C20-(2 h), C30-(2 h), and C40-(2 h) compared with their pairs without pre-curing, respectively.

3.4. Compressive strength

3.4.1. Effects of CSABF cement content on the strength development of freezer-cured pastes

Replacing PC with CSABF cement enhanced the early and late compressive strengths of the freezer-cured pastes (−5 °C) (Fig. 7). A negligible strength development was reported in the C0-(0 h) paste. This finding is mainly caused by the freezing of pore solution (see Table 3), which suppresses the hydration process and formation of strength-bearing reaction products. Therefore, no compressive strength could be measured in the 1d-old C0-(0 h) paste, and only 8 MPa were reported after 90 days. Early strength development was significantly enhanced when the CSABF cement content was ≥30 wt%. Thus, both the one-day-old C30-(0 h) and C40-(0 h) gained approximately 11.4 MPa. Thereafter, a very limited strength gain was noticed between 1 and 28 days of the curing period when the CSABF cement content was ≥30 wt%. This result can be attributed to the deaccelerating effects of high CSABF cement content (increased amount of released aluminum ions) on the hydration of alite and belite phases in the PC fraction, as described later in Section 3.5. Nevertheless, the compressive strengths of the 90-day-old freeze-cured pastes increased to 15.3, 20.6, 76.5, and 40.6 MPa in C10-(0 h), C20-(0 h), C30-(0 h), and C40-(0 h), respectively. The significant increase in the compressive strength of the C30 binder after 28 days is attributed to the enhanced precipitation of pore-filling amorphous phases (C–S–H, AH_3, and AFm) due to the ongoing hydration of alite and ye'elimite (see Fig. 10[a, d, and g] in Section 3.5) [7,49,50]. When CSABF cement content increased up to 40% in C40-(0 h), lower compressive strengths were reported from 7 days onwards compared with that in C30-(0 h). This finding is mainly associated with the porosity of the microstructure, as shown later in Section 3.6.1. Therefore, 30 wt% CSABF cement content is the optimal replacement level for the materials used in this study.

Table 3
Freezing points (°C) of the binders with and without the 2 h pre-curing interval.

Pre-curing period (h)	Mix composition				
	C0	C10	C20	C30	C40
0	−1.3	−2.9	−3.5	−5.3	−5.5
2	−1.4	−4.1	−5.7	−6.2	−6.7

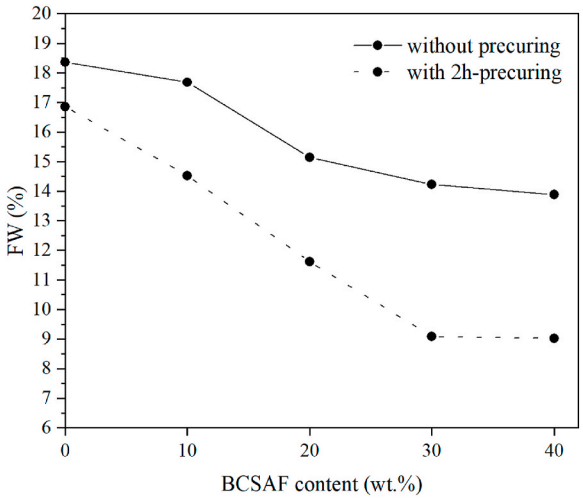

Fig. 6. Effects of CSABF content and 2 h pre-curing period at room temperature on the amount of freezable water (i.e., the melting heat) of the binders.

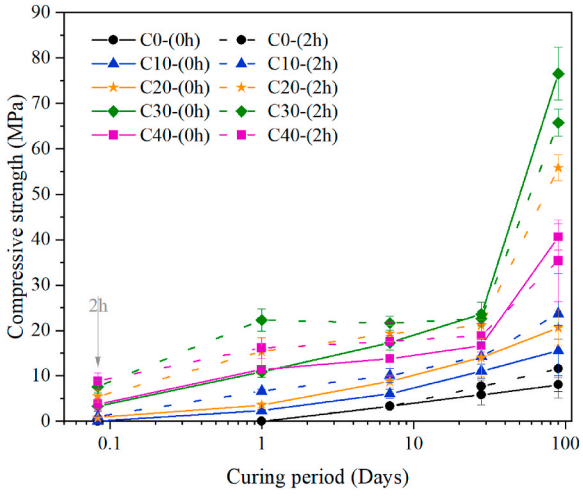

Fig. 7. The impacts of CSABF content and pre-curing treatment on the compressive strength of freezer-cured pastes (−5 °C).

The frozen C0-(0 h), C10-(0 h), and C20-(0 h) showed strength development with time, which can be assigned to the ongoing hydration reaction by unfrozen pore solution trapped in nano-sized pores. Previously, Liu et al. [51] and Beddoe and Setzer [52] proved that the freezing point of pore solution in gel nano-sized can be depressed from −23 °C to −38 °C, depending on pore size. Subsequently, this supercooled pore solution can further dissolve cement particles and react with them in the small pores; however, at a slow rate, precipitation of hydration products is increased. In addition, the ongoing dissolution of anhydrous cement particles increased the ion concentration in the small pores, which created a concentration gradient between pores. As a result, the unfrozen highly concentrated pore solutions in the small pores begin to migrate to ice-bodies in large capillary pores until equilibrium is reached [53–55]. Consequently, ice in large pores starts to melt due to increased ion concentration [42,43]. The latter provides the needed liquid-state pore solution for the subsequent hydration process and reaction product formation, which illustrates the detected compressive strength development in the frozen pastes.

When the 2 h pre-curing period was provided, the strength development of PC/CSABF pastes was significantly accelerated, while limited enhancements were observed in C0-(2 h). According to the results, the impacts of the 2 h pre-curing interval on compressive strength are highly dependent on CSABF cement content and curing time. For instance, with low CSABF cement content (i.e., 10 and 20 wt%), both early and late compressive strengths were enhanced with the 2 h pre-curing period. Therefore, 1- and 90-day-old compressive strengths of C10-(2 h) were increased by approximately 279% (6.7 MPa) and 52.9% (23.7 MPa) compared with their counterparts without pre-curing. Similarly, with the 20 wt% CSABF content, both the 1 day and 90 days compressive strengths of C20-(2 h) were increased to approximately 15.3 and 55.8 MPa, which are 4.3 and 2.7 times higher than those measured in the 1 day- and 90-day-old C20-(0 h) samples, respectively. This finding can be explained by the decreased freezing point of the C10 and C20 binders with the 2 h pre-curing period (see Table 3), which reduces the freezing cracking risk and assures the availability of the needed liquid-state pore solution for the follow-up hydration process. When the CSABF content was increased to 30 and 40 wt%, the 2 h pre-curing interval improved the strength development during the first 7 days and diminished thereafter in comparison with their pairs cured without pre-curing. For instance, the 1-day-old C30-(2 h) (22.3 MPa) and C40-(2 h) (16.2 MPa) gained 2.2 and 1.6 times higher compressive strengths than C30-(0 h) and C40-(0), respectively. By contrast, the 90-day-old compressive strengths of C30-(2 h) (65.8 MPa) and C40-(2 h) (35.3 MPa) were 14% and 18% lower than those of C30-(0 h) and C40-(0 h), respectively. The latter can be assigned to the rapid early AFt precipitation, which increased the loose and porous microstructure at a late age, as shown later in Section 3.6.2.

3.4.2. *Effects of natural winter conditions on strength development of the C30 paste*

The best performing binder (i.e., C30), in terms of compressive strength measurements, was selected to assess the impacts of natural Finnish winter conditions on strength development up to 12 months (Fig. 8). Notably, no special precautions or thermal systems were used during the outdoor curing period. Promisingly, the externally cured C30 binder gained compressive strength with time despite the severe drop in the ambient temperature up to −23 °C (see Fig. A2 in Appendix A) and regardless of the pre-curing conditions. However, the compressive strength gain rate was slower in the externally cured samples than that in the freezer-cured samples (−5 °C) during the first 90 days, regardless of the pre-curing treatment (Fig. 9). Therefore, lower compressive strengths were gained in the externally cured C30 samples compared with those in the freezer-cured pairs during the first 90 days of the curing period. The latter can be attributed to the lower ambient temperatures (Fig. A2) than the freezer temperature (−5 °C), which decelerate the hydration rate of the precursors and may also freeze a portion of pore solution, thus further slowing down the hydration process rate, diminishing the rate and amount of precipitated strength-giving phases. Promisingly, with increased ambient temperature from 120 days onwards, the strength development rate was considerably accelerated. As a result, the externally cured 360-day-old C30-(0 h) (≈93 MPa) and C30-(2 h) (≈81 MPa) gained higher compressive strengths than those measured in their 90-day-old freezer-cured pairs. The compressive strength development of the externally cured samples indicates that the C30 binder, regardless of the pre-curing period, rapidly developed a strong microstructure at an early age, which can withstand any potential increase in internal hydraulic stress due to the freezing of capillary pore solution because of the severe drop in ambient temperatures. The American Concrete Institute [56] recommends that fresh concrete elements must be protected against freezing until a compressive strength of 5 MPa was gained to be able to withstand a subsequent early freezing risk. According to the results, 8 and 17 MPa were gained in the 1-day-old externally cured C30-(0 h) and C30-(2 h) samples.

3.5. *Reaction product evolution*

The mineralogical composition was assessed by Q-XRD (Fig. 10) and TGA/DTG analysis (Fig. 11). The XRD analysis (see Fig. A4) shows that alite (C_3S), belite (C_2S), ye'elimite ($C_4A_3\$$), portlandite (CH), and AFt are the main crystalline phases in the C10 and C30 binders, and their quantities, as well as the content of amorphous phases, were then calculated by the Rietveld refinement analysis. The amounts of ferrite phase were under the reliable detection limit of XRD and were excluded from the analysis. Moreover, the TGA/DTG analysis was used to differentiate between the precipitated amorphous hydrates and to further confirm the Q-XRD results.

In the low CSABF content binder (i.e., C10), ye'elimite was consumed with time (Fig. 10 [a]). With the hydration of ye'elimite in the presence of gypsum, AFt was formed and reached its maximum content at 28 and 7 days in C10-(0 h) and C10-(2 h), respectively (Fig. 10 [c]). The latter indicates that the precuring period accelerated the reaction between ye'elimite and gypsum in the C10 binder. Therefore, gypsum still existed up to 28 days in C10-(0 h), whereas it was entirely consumed within 7 days in C10-(2 h) (Fig. 10 [b]). Moreover, the amount of AFt in 1-day-old C10-(2 h) was 43% higher than that in C10-(0 h). When the content of CSABF was increased to 30 wt%, the amount of ye'elimite was sharply decreased during the first 2 h. Meanwhile, the AFt phase was rapidly generated and reached its maximum content at 2 h, regardless of

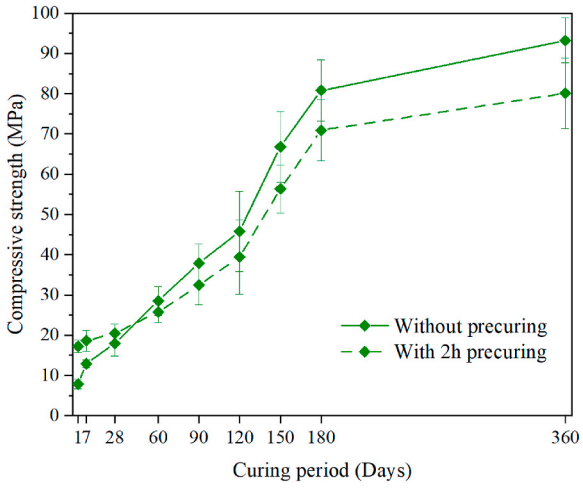

Fig. 8. One-year strength development of C30 binder cured under external conditions (with and without the 2 h pre-curing period). The casting date was Dec. 17, 2020, and the ambient temperature was −5.3 °C at the time of casting. The temperatures represent the lowest and highest ambient temperatures in each curing month.

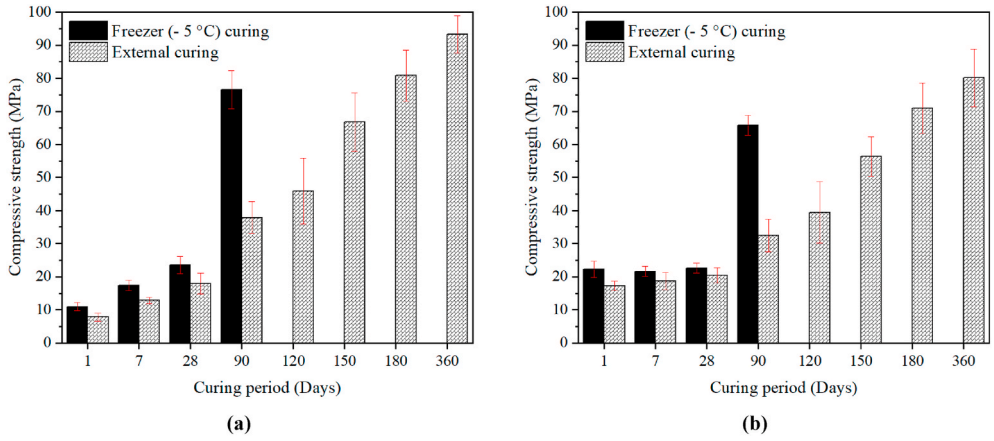

Fig. 9. Comparison between freezer-cured and external-cured C30 pastes: (a) without and (b) with the 2 h pre-curing period.

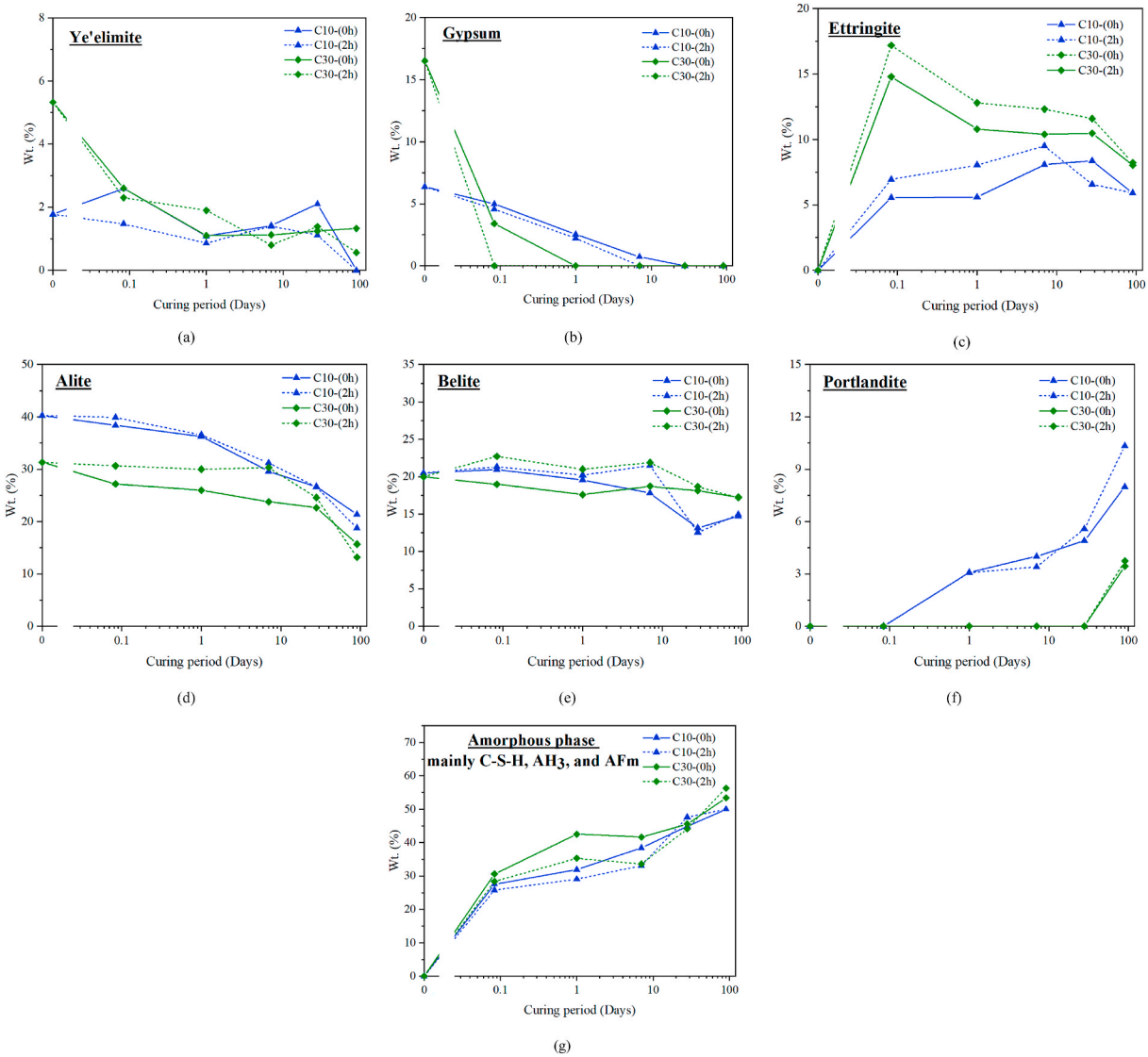

Fig. 10. Trend lines of QXRD analysis (normalized to 100 g of paste): (a) ye'elimite, (b) gypsum, (c) ettringite, (d) alite, (e) belite, (f) portlandite, and (g) amorphous phase "the amorphous content was measured using 20 wt% TiO_2 and because of the background of XRD analysis it only shows the content trend and not the actual value." The origin (0,0) in the charts shows the initial values of the studied phases. The R_{wp} of the analyses were between 3 and 5%.

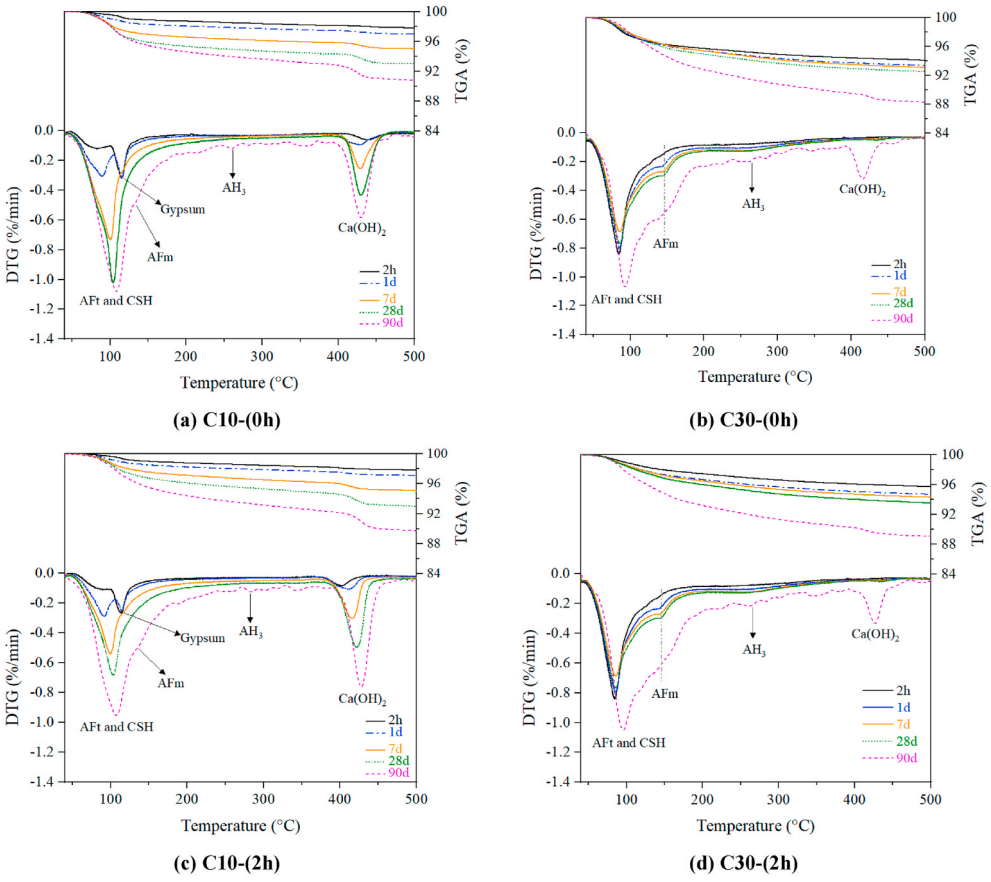

Fig. 11. TGA/DTG curves of C10 and C30 pastes.

the pre-curing period. Thus, the 2 h old C30 binder formed 2.5 times higher amounts of AFt than the C10 binder, regardless of the precuring period. This result shows that the early hydration and precipitation of early strength-source AFt are more violent with increasing CSABF cement content. The latter is in line with the compressive strength results, as shown in Fig. 7 in Section 3.4.1.

The hydration of alite and belite phases was retarded in the PC/CSABF binders and more significantly in the binder with a high content of BCSA cement (i.e., C30). Regarding the alite phase, the hydration process started after the first curing day in the C10 binder (Fig. 10 [d]). As a result, the portlandite phase started to form and increased from 1 day onwards in the C10 binder, indicating the formation of C–S–H and continuous hydration of the alite phase (Fig. 10 [f] and Fig. 11 [a and c]). In comparison with the C10 binder, the hydration of the alite phase in C30 was considerably slower and only started after 28 days, regardless of the pre-curing period. This result is consistent with the early absence of the portlandite phase in the C30 binders and its appearance after 28 days, regardless of the precuring period. Similarly, the reactivity of the belite phase was low at all hydration times and slower in rate than the alite phase (Fig. 10 [e]).

Furthermore, the short precuring period has no impact on the hydration rate of calcium silicate phases (i.e., alite and belite), regardless of the CSABF cement content. Nevertheless, the delayed hydration rate of alite and belite phases can be attributed to the inhibiting impact of the rapid early hydration of CSABF cement and consumption of a large amount of water by AFt formation, as shown in Eqs. (2)–(4) [57]. In addition, Damidot and Rettel [58] and Ben Haha et al. [59] previously investigated the impacts of aluminates on the hydration of alite and belite phases. They showed that the hydration and dissolution of calcium silicate phases were inhibited by the high alumina concentration in the pore solution due to the "poison effect" of [Al] on the nucleation of C–S–H. Moreover, the low w/c ratio (i.e., 0.27) used in this study, along with the extensive consumption of water by the hydration of the rapid reactive phases (i.e., $C_4A_3\$$, C_3A, $C_{12}A_7$, and C_3S), have further diminished the reactivity of C_2S phase, especially in the C30 binder. Therefore, expectedly, the precipitated C–S–H gel and portlandite in the C30 blend are a result of alite hydration only; however, their formation in the C10 blend can be attributed to the hydration of alite and belite phases. Based on the abovementioned observations, the initial and early hydration processes and strength development in the PC/CSABF paste are mainly controlled by the reactivity of the calcium aluminate phases (i.e., $C_4A_3\$$, C_3A, and $C_{12}A_7$), and the late hydration and strength gain are attributed to the hydration of calcium silicate phases (i.e., C_3S and C_2S).

Furthermore, the X-ray amorphous phases (i.e., AFm, AH_3, and C–S–H) show an increasing trend with time (Fig. 10 [g]). Fig. 11 shows that the content of the AFm phase was increased with time as a result of ongoing hydration of ye'elimite in the absence of gypsum (Eq. (6)) and partial destabilization of AFt with depletion of available sulfate. In addition, as shown in Eqs. (2) and (5), the second hydration product of the ye'elimite phase is microcrystalline AH_3 that is generally X-ray amorphous [59,60]. The AH_3 hydration product was detected in the C10 and C30 samples, and its amount was increased with time, as demonstrated by TGA/DTG results. The latter can be attributed to the ongoing hydration of unreacted ye'elimite in the absence of gypsum. Moreover, the detected increase in the amorphous content can also be attributed to the increased amount of precipitated C–S–H as a result of the hydration progress of calcium silicate phases with time.

$$C_4A_3\$ + 18\ H \rightarrow C_4A\$H_{12} + 2\ AH_3 \quad (5)$$

3.6. Microstructural characterization

3.6.1. SEM

The microstructures of the 90-day-old freezer-cured C10, C30, and

C40 pastes without pre-curing are shown in Fig. 12. The matrices consist of voids, hydration products, and residual PC and CSABF clinker particles (in order of lowest brightness to highest brightness in BSE images). Attributing to the high freezing point (−2.9 °C, see Table 3) of C10-(0 h), its microstructure was fractured, and large and connected voids were detected as a result of frost damage. When the CSABF cement content was increased to 30%, the microstructure of C30-(0 h) looked intact, dense, and filled with a considerable amount of hydration products. Nevertheless, large voids and cracks were observed in the microstructure of the C40-(0 h) as a result of very rapid crystallization and precipitation of AFt. The latter can explain the lower compressive strength of the 90-day-old C40-(0 h) sample compared with that of the 90-day-old C30-(0 h) sample, as shown earlier in Section 3.4.1.

3.6.2. MIP

The total porosity of the binder decreased with an increase in curing time and CSABF cement content (Fig. 13). The highest porosity was detected in the C10-(0 h) sample cured for 1 day and is mainly attributed to frost damage and a low amount of precipitated pore-filling hydration products. With increasing CSABF cement content in the C30-(0 h) sample, at 1 day of curing, the porosity was decreased as a result of the enhanced precipitation of AFt and amorphous phases that fill the paste matrix. Moreover, the impacts of the 2 h pre-curing period on the porosity of the PC/CSABF samples are dependent on CSABF cement content and sample age. At low CSABF cement content (i.e., 10 wt), the 2 h pre-curing period decreased the 1- and 90-day porosities due to the increased precipitation of the hydration products, as shown earlier in Section 3.5. Similarly, the 2 h pre-curing period decreased the 1-day porosity in the C30 paste. However, in the 90-day-old C30 paste, porosity increased with the pre-curing period. This finding is consistent with the compressive strength results (Fig. 7) and is likely due to the rapid AFt precipitation during the precuring that covers the cement particles, thus limiting the late hydration process and reducing the amount of pore-filling hydration products (see Fig. 11 [b] and [d]).

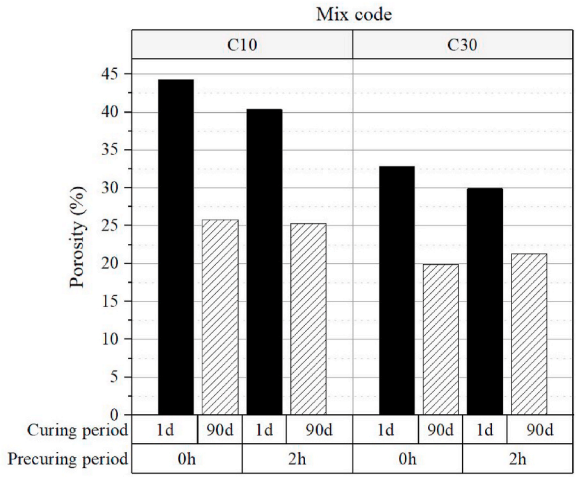

Fig. 13. Total porosity of selected hardened pastes.

4. Conclusion

This work aims to develop an environmentally friendly binder that can harden at subzero curing conditions, extend the construction season in cold regions, and decrease the environmental load of cold weather concreting works. An eco-friendly CSABF cement manufactured using industrial side streams (i.e., ladle slag, iron-slag, and phosphogypsum) was used to accelerate the strength development of PC-based paste cured in a freezer at −5 °C or under natural winter conditions, with and without the 2 h pre-curing period at room temperature.

The use of the CSABF cement accelerates the hydration rate and setting time of the paste, and the acceleration rate is directly proportional to the CSABF cement content. The incorporation of CSABF cement (≥30 wt%) reduces the paste's freezing point to below −5 °C as a result of concentration and network effects, regardless of the pre-curing period. Simultaneously, the amount of freezable water (FW) in the PC/CSABF paste is decreased because of the accelerated hydration rate and consumption of free water on the part of the precipitated hydration products. The freezing point and FW amount of binders are further decreased with the 2 h pre-curing period at room temperature, regardless of the CSABF content.

The incorporation of CSABF cement enhances the compressive strength of pastes cured at −5 °C. In the presence of the optimal dosage (i.e., 30 wt%) of CSABF cement, the 90-day-old PC/CSABF paste can gain 5 times higher compressive strength than the 100% PC-based binder. A further increase in the content of CSABF cement (>30 wt%) leads to a porous microstructure and a reduction in compressive strength. The impacts of pre-curing at room temperature on the early and late compressive strengths and microstructure porosity are dependent on the CSABF cement content and curing period. The early gained compressive strengths in the PC/CSABF pastes are attributed to the rapid precipitation of AFt, whereas the late strength development is controlled by the hydration of alite and belite phases. The 180-day-old outdoor-cured 70%PC/30CSABF binder gains a comparable compressive strength, similar to that measured in the 90-day-old freezer-cured pair, despite the severe drop in ambient temperature to below −20 °C. The findings of this study exhibit the potential use of CSABF cement as an eco-friendly accelerator in cold-weather construction works.

Author contribution

Ahmad Alzaza: Conceptualization, data curation, formal analysis, investigation, methodology, validation, visualization, writing—original draft, and writing—review, and editing. **Katja Ohenoja:** Conceptualization, methodology, formal analysis, validation, visualization, writing—review, and editing, supervision, and funding acquisition. **Visa Isteri:** Data curation, formal analysis, investigation, methodology, validation, visualization, and writing—review, and editing. **Theodore Hanein:** validation and writing—review, and editing. **Daniel Geddes:**

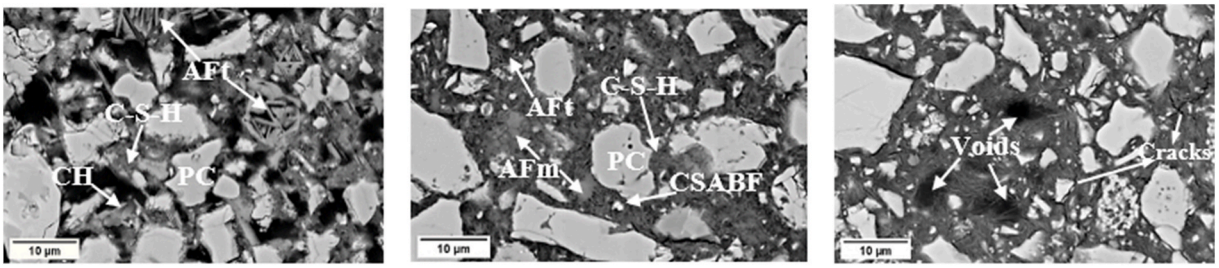

Fig. 12. Microstructures of the 90-day-old freezer-cured pastes (5000× magnification).

Investigation, methodology, validation, visualization, and writing—review, and editing. **Minna Poikelispää:** Validation and writing—review, and editing. **Mirja Illikainen:** Conceptualization, resources, visualization, writing—review, editing, supervision, and funding acquisition.

Funding

This work was conducted under the auspices of the ARCTIC-ecocrete project, which was supported by the Interreg Nord EU program and the Regional Council of Lapland, and the CECIRE project, which was funded by Business Finland and the Finnish companies Boliden Harjavalta, Boliden Kokkola, Outokumpu Stainless, and Yara and Fortum Waste Solutions.

Declaration of competing interest

The authors declare that they have no known competing financial interests or personal relationships that could have appeared to influence the work reported in this paper.

Acknowledgments

Mr. Jarno Karvonen and Mr. Tun Nyo are acknowledged for their contributions to the laboratory work. Mr. Petri Manninen (Sika, Finland) and Mr. Esa Heikkilä (Finnsementti, Finland) are acknowledged for providing materials for this study. The authors thank the Center for Material Analysis, University of Oulu, Finland. We also thank Tauno Tönning Foundation for the financial support of the work. Participation of Theodore Hanein was funded by UKRI FLF (MR/V023829/1).

Appendix A

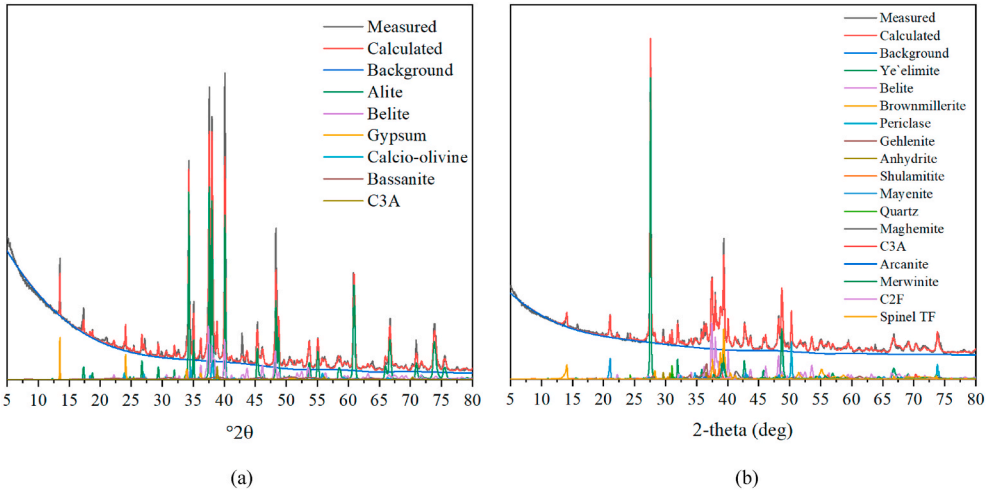

Fig. A1. QXRD of (a) PC and (b) CSABF clinker with phase identification and intensities calculated with the Rietveld method. Blackline represents the measured diffractogram, redline refers to the measured intensities, and identified phases are listed in (Table 1).

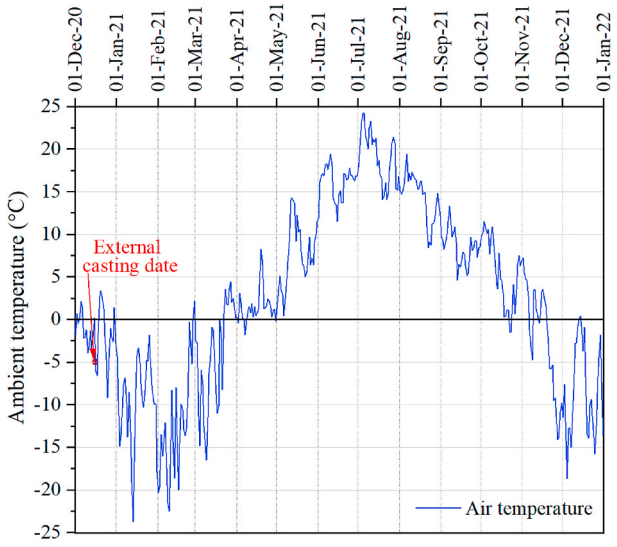

Fig. A2. Average air temperature (°C) during the external curing period (Finnish Meteorological Institute [61]).

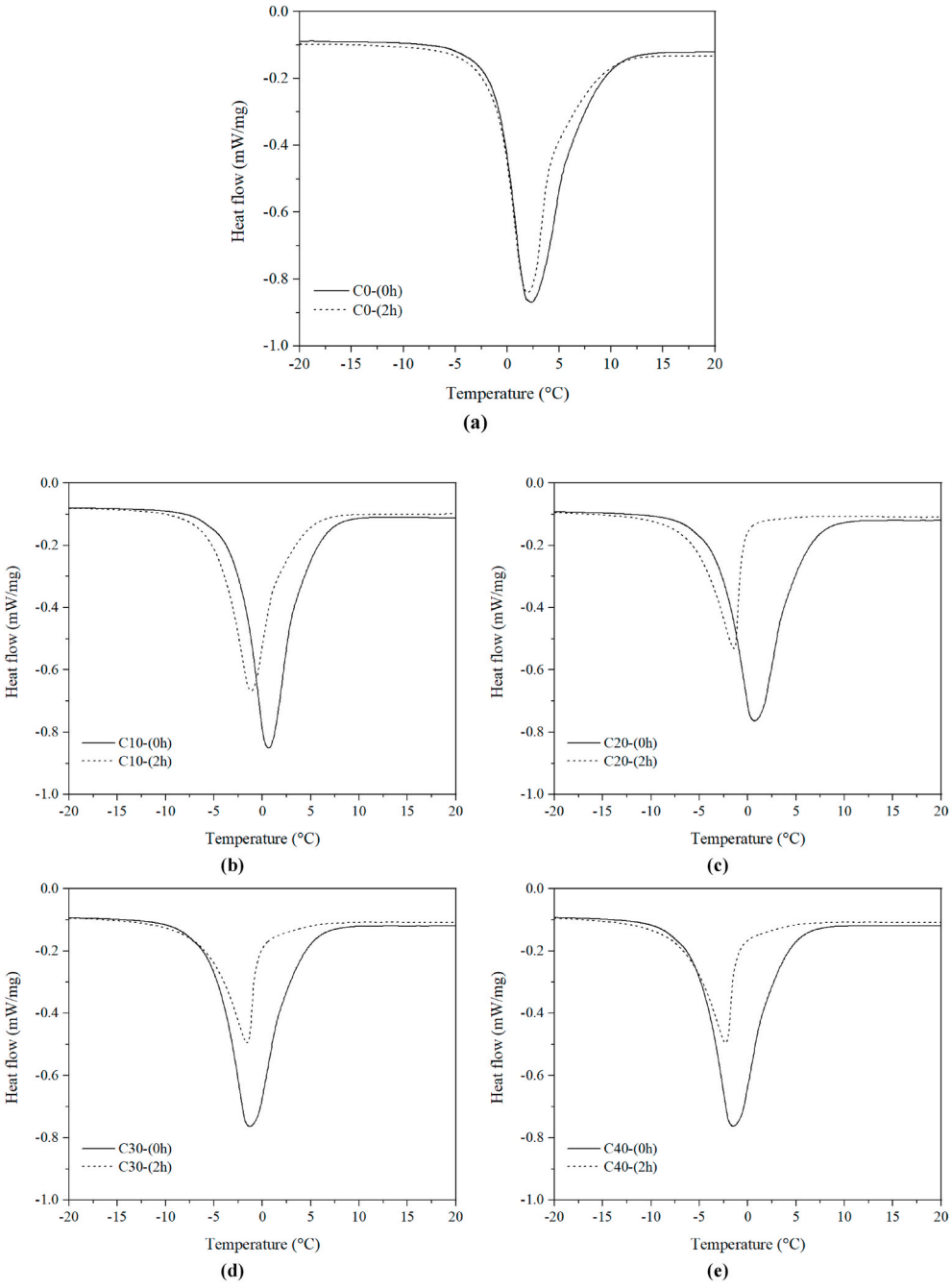

Fig. A3. LT-DSC heat flow curves of (a) C0; (b) C10; (c) C20; (d) C30; and (e) C40 with and without the 2 h pre-curing period at 22 ± 1 °C. The time between parentheses represents the pre-curing period.

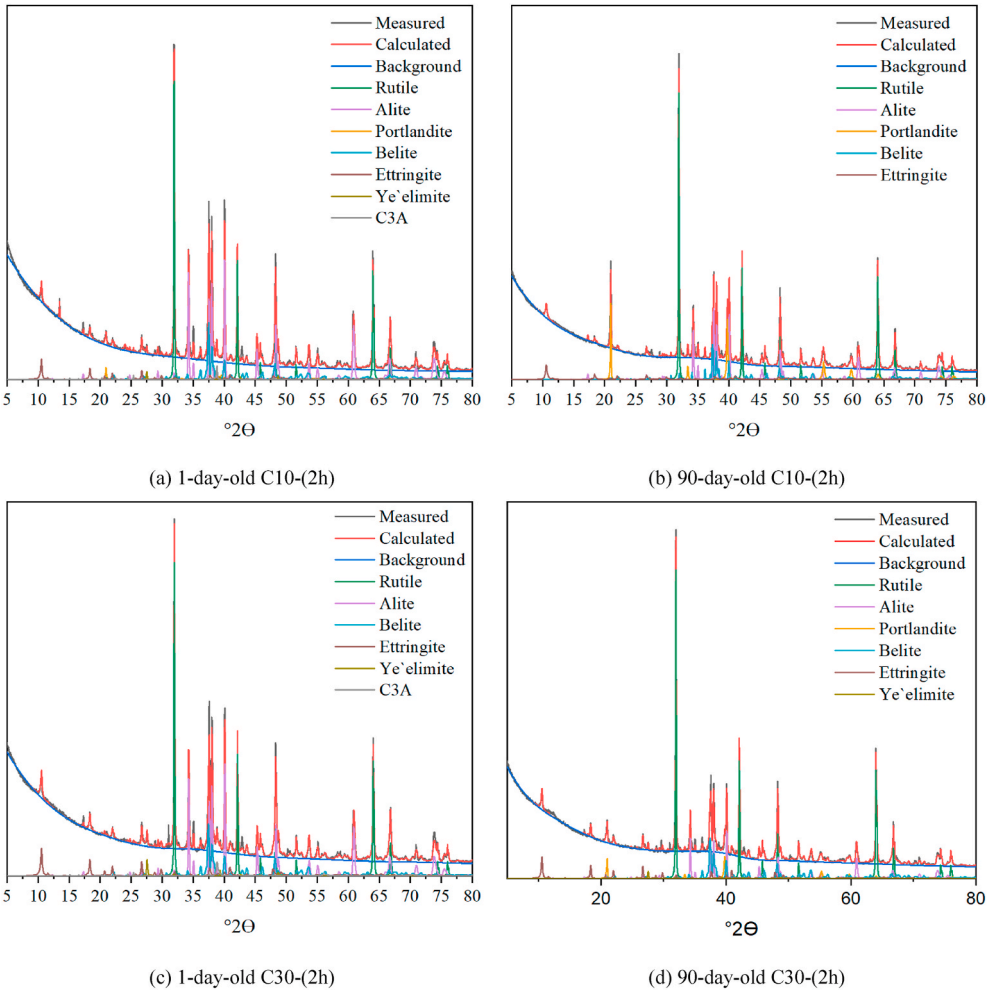

Fig. A4. XRD patterns of the selected samples with internal standard (i.e., TiO_2).

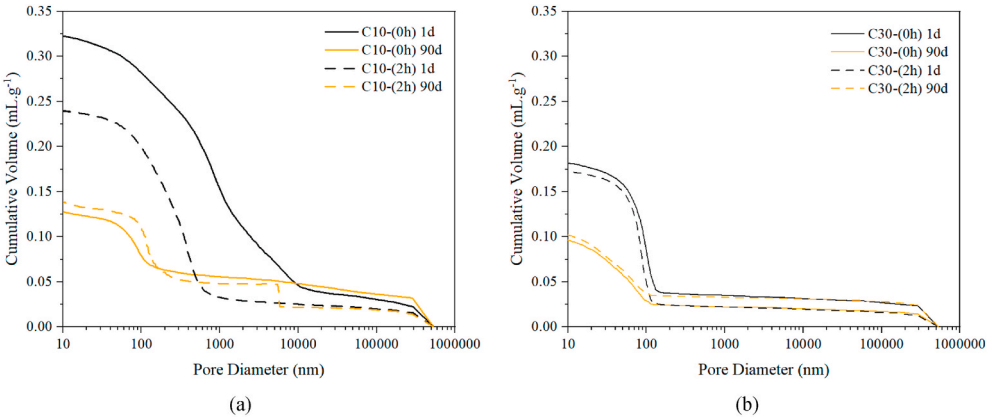

Fig. A5. Pore size distribution curves of (a) C10 and (b) C30, showing the effects of CSABF cement content, precuring period, and curing period.

References

[1] G. Huang, D. Pudasainee, R. Gupta, W. Victor Liu, Hydration reaction and strength development of calcium sulfoaluminate cement-based mortar cured at cold temperatures, Construct. Build. Mater. 224 (2019) 493–503, https://doi.org/10.1016/j.conbuildmat.2019.07.085.

[2] P. Li, X. Gao, K. Wang, V.W.Y. Tam, W. Li, Hydration mechanism and early frost resistance of calcium sulfoaluminate cement concrete, Construct. Build. Mater. 239 (2020), 117862, https://doi.org/10.1016/j.conbuildmat.2019.117862.

[3] J. Liu, Y. Li, Y. Yang, Y. Cui, Effect of low temperature on hydration performance of the complex binder of silica fume-portland cement, J. Wuhan Univ. Technol.-Materials Sci. Ed. 29 (2014) 75–81, https://doi.org/10.1007/s11595-014-0870-2.

[4] C.J. Korhonen, Antifreeze Admixtures for Cold Regions Concreting: a Literature Review, Cold Regions Research and Engineering Lab Hanover NH, 1990. https://apps.dtic.mil/sti/pdfs/ADA228559.pdf.

[5] F. Karagöl, R. Demirboğa, M.A. Kaygusuz, M.M. Yadollahi, R. Polat, The influence of calcium nitrate as antifreeze admixture on the compressive strength of concrete exposed to low temperatures, Cold Reg. Sci. Technol. 89 (2013) 30–35, https://doi.org/10.1016/j.coldregions.2013.02.001.

[6] L. Qin, X. Gao, A. Zhang, Potential application of Portland cement-calcium sulfoaluminate cement blends to avoid early age frost damage, Construct. Build. Mater. 190 (2018) 363–372, https://doi.org/10.1016/j.conbuildmat.2018.09.136.

[7] G. Zhang, Y. Yang, H. Yang, H. Li, Calcium sulphoaluminate cement used as mineral accelerator to improve the property of Portland cement at sub-zero temperature, Cement Concr. Compos. 106 (2020), 103452, https://doi.org/10.1016/j.cemconcomp.2019.103452.

[8] E. Gartner, Industrially interesting approaches to "low-CO2" cements, Cement Concr. Res. 34 (2004) 1489–1498, https://doi.org/10.1016/j.cemconres.2004.01.021.

[9] E. Gartner, K. Quillin, Low-CO2 Cements Based on Calcium Sulfoaluminates, 2007.

[10] E. Gartner, H. Hirao, A review of alternative approaches to the reduction of CO2 emissions associated with the manufacture of the binder phase in concrete, Cement Concr. Res. 78 (2015) 126–142, https://doi.org/10.1016/j.cemconres.2015.04.012.

[11] E.M. Gartner, D.E. Macphee, A physico-chemical basis for novel cementitious binders, Cement Concr. Res. 41 (2011) 736–749, https://doi.org/10.1016/j.cemconres.2011.03.006.

[12] L. Xu, K. Wu, N. Li, X. Zhou, P. Wang, Utilization of flue gas desulfurization gypsum for producing calcium sulfoaluminate cement, J. Clean. Prod. 161 (2017) 803–811, https://doi.org/10.1016/j.jclepro.2017.05.055.

[13] A. Telesca, M. Marroccoli, M.L. Pace, M. Tomasulo, G.L. Valenti, P.J.M. Monteiro, A hydration study of various calcium sulfoaluminate cements, Cement Concr. Compos. 53 (2014) 224–232, https://doi.org/10.1016/j.cemconcomp.2014.07.002.

[14] A. Telesca, M. Marroccoli, M. Tomasulo, G. Valenti, S. Allevi, M. Marchi, Microstructural features and technical properties of calcium sulfoaluminate based cements, in: Proc. First Int. Conf. Sulphoaluminate Cem. Mater. Eng. Technol. Wuhan China, 2013.

[15] J.J. Wolf, D. Jansen, F. Goetz-Neunhoeffer, J. Neubauer, Mechanisms of early ettringite formation in ternary CSA–OPC–anhydrite systems, Adv. Cement Res. 31 (2018) 195–204, https://doi.org/10.1680/jadcr.18.00115.

[16] Y. Huang, J. Qian, X. Kang, J. Yu, Y. Fan, Y. Dang, W. Zhang, S. Wang, Belite-calcium sulfoaluminate cement prepared with phosphogypsum: influence of P2O5 and F on the clinker formation and cement performances, Construct. Build. Mater. 203 (2019) 432–442, https://doi.org/10.1016/j.conbuildmat.2019.01.112.

[17] V. Isteri, K. Ohenoja, T. Hanein, H. Kinoshita, H. Kletti, C. Rößler, P. Tanskanen, M. Illikainen, T. Fabritius, Ferritic calcium sulfoaluminate belite cement from metallurgical industry residues and phosphogypsum: clinker production, scale-up, and microstructural characterisation, Cement Concr. Res. 154 (2022), 106715, https://doi.org/10.1016/j.cemconres.2022.106715.

[18] I.A. Chen, M.C.G. Juenger, Incorporation of coal combustion residuals into calcium sulfoaluminate-belite cement clinkers, Cement Concr. Compos. 34 (2012) 893–902, https://doi.org/10.1016/j.cemconcomp.2012.04.006.

[19] X. Guo, H. Shi, W. Hu, K. Wu, Durability and microstructure of CSA cement-based materials from MSWI fly ash, Cement Concr. Compos. 46 (2014) 26–31, https://doi.org/10.1016/j.cemconcomp.2013.10.015.

[20] M.L. Pace, A. Telesca, M. Marroccoli, G.L. Valenti, Use of industrial byproducts as alumina sources for the synthesis of calcium sulfoaluminate cements, Environ. Sci. Technol. 45 (2011) 6124–6128, https://doi.org/10.1021/es2005144.

[21] S. Sahu, J. Majling, Preparation of sulphoaluminate belite cement from fly ash, Cement Concr. Res. 24 (1994) 1065–1072, https://doi.org/10.1016/0008-8846(94)90030-2.

[22] V. Petkova, V. Stoyanov, Y. Pelovski, TG–DTG–DTA in studying white self-compacting cement mortars, J. Therm. Anal. Calorim. 109 (2012) 797–806, https://doi.org/10.1007/s10973-012-2447-7.

[23] A. Alzaza, K. Ohenoja, I. Langås, B. Arntsen, M. Poikelispää, M. Illikainen, Low-temperature (−10 °C) curing of Portland cement paste – synergetic effects of chloride-free antifreeze admixture, C–S–H seeds, and room-temperature pre-curing, Cement Concr. Compos. (2021), 104319, https://doi.org/10.1016/j.cemconcomp.2021.104319.

[24] A. Alzaza, K. Ohenoja, M. Illikainen, One-part alkali-activated blast furnace slag for sustainable construction at subzero temperatures, Construct. Build. Mater. 276 (2021), 122026, https://doi.org/10.1016/j.conbuildmat.2020.122026.

[25] A. Alzaza, K. Ohenoja, M. Illikainen, Improved strength development and frost resistance of Portland cement ground-granulated blast furnace slag binary binder cured at 0 °C with the addition of calcium silicate hydrate seeds, J. Build. Eng. 48 (2022) 103904, https://doi.org/10.1016/j.jobe.2021.103904.

[26] EN196-3, Methods for Testing Cement: Part 3. Determination of Setting Time and Soundness, CEN, Brussels, 2016.

[27] S. Zhang, Y. Zhao, H. Ding, J. Qiu, C. Hou, Effect of sodium chloride concentration and pre-curing time on the properties of cemented paste backfill in a sub-zero environment, J. Clean. Prod. 283 (2021), 125310, https://doi.org/10.1016/j.jclepro.2020.125310.

[28] A. Damasceni, L. Dei, E. Fratini, F. Ridi, S.-H. Chen, P. Baglioni, A novel approach based on differential scanning calorimetry applied to the study of tricalcium silicate hydration kinetics, J. Phys. Chem. B 106 (2002) 11572–11578, https://doi.org/10.1021/jp020211l.

[29] E. Xanthakis, A. Le-Bail, H. Ramaswamy, Development of an innovative microwave assisted food freezing process, Innovat. Food Sci. Emerg. Technol. 26 (2014) 176–181, https://doi.org/10.1016/j.ifset.2014.04.003.

[30] A. Alzaza, K. Ohenoja, M. Illikainen, Enhancing the mechanical and durability properties of subzero-cured one-part alkali-activated blast furnace slag mortar by using submicron metallurgical residue as an additive, Cement Concr. Compos. (2021), 104128, https://doi.org/10.1016/j.cemconcomp.2021.104128.

[31] J. Zhang, G.W. Scherer, Comparison of methods for arresting hydration of cement, Cement Concr. Res. 41 (2011) 1024–1036, https://doi.org/10.1016/j.cemconres.2011.06.003.

[32] Q. Zeng, K. Li, T. Fen-Chong, P. Dangla, Analysis of pore structure, contact angle and pore entrapment of blended cement pastes from mercury porosimetry data, Cement Concr. Compos. 34 (2012) 1053–1060, https://doi.org/10.1016/j.cemconcomp.2012.06.005.

[33] Z. He, Y. Li, The influence of mayenite employed as a functional component on hydration properties of ordinary portland cement, Materials 11 (2018), https://doi.org/10.3390/ma11101958.

[34] G. Le Saoût, B. Lothenbach, A. Hori, T. Higuchi, F. Winnefeld, Hydration of Portland cement with additions of calcium sulfoaluminates, Cement Concr. Res. 43 (2013) 81–94, https://doi.org/10.1016/j.cemconres.2012.10.011.

[35] L. Zhang, F.P. Glasser, Hydration of calcium sulfoaluminate cement at less than 24 h, Adv. Cement Res. 14 (2002) 141–155, https://doi.org/10.1680/adcr.2002.14.4.141.

[36] P. Chaunsali, P. Mondal, Hydration and early-age expansion of calcium sulfoaluminate cement-based binders: experiments and thermodynamic modeling, J. Sustain. Cem.-Based Mater. 5 (2016) 259–267, https://doi.org/10.1080/21650373.2015.1060184.

[37] K. Gijbels, H. Nguyen, P. Kinnunen, W. Schroeyers, Y. Pontikes, S. Schreurs, M. Illikainen, Feasibility of incorporating phosphogypsum in ettringite-based binder from ladle slag, J. Clean. Prod. 237 (2019), 117793, https://doi.org/10.1016/j.jclepro.2019.117793.

[38] S. Park, Y. Jeong, J. Moon, N. Lee, Hydration characteristics of calcium sulfoaluminate (CSA) cement/portland cement blended pastes, J. Build. Eng. 34 (2021), 101880, https://doi.org/10.1016/j.jobe.2020.101880.

[39] H.F.W. Taylor, Cement Chemistry, second ed., T. Telford, London, 1997.

[40] C.W. Hargis, B. Lothenbach, C.J. Müller, F. Winnefeld, Further insights into calcium sulfoaluminate cement expansion, Adv. Cement Res. 31 (2019) 160–177, https://doi.org/10.1680/jadcr.18.00124.

[41] H. Nguyen, W. Kunther, K. Gijbels, P. Samyn, V. Carvelli, M. Illikainen, P. Kinnunen, On the retardation mechanisms of citric acid in ettringite-based binders, Cement Concr. Res. 140 (2021), 106315, https://doi.org/10.1016/j.cemconres.2020.106315.

[42] F.-M. Raoult, Loi générale des tensions de vapeur des dissolvants, C. R. Hebd. Seances Acad. Sci. 104 (1887) 1430–1433.

[43] É. Clapeyron, Mémoire sur la puissance motrice de la chaleur, J. LÉcole Polytech. 14 (1834) 153–190.

[44] G. Zhang, Y. Yang, H. Li, Calcium-silicate-hydrate seeds as an accelerator for saving energy in cold weather concreting, Construct. Build. Mater. 264 (2020), 120191, https://doi.org/10.1016/j.conbuildmat.2020.120191.

[45] M. Chai, J. Zhang, H. Zhang, Y. Mu, G. Sun, Z. Yin, A method for calculating unfrozen water content of silty clay with consideration of freezing point, Appl. Clay Sci. 161 (2018) 474–481, https://doi.org/10.1016/j.clay.2018.05.015.

[46] B.R. Puri, L.R. Sharma, M.L. Lakhanpal, Freezing point of water held in porous bodies at different vapor pressures, J. Phys. Chem. 58 (1954) 289–292, https://doi.org/10.1021/j150514a001.

[47] P. Pipilikaki, M. Beazi-Katsioti, The assessment of porosity and pore size distribution of limestone Portland cement pastes, Construct. Build. Mater. 23 (2009) 1966–1970, https://doi.org/10.1016/j.conbuildmat.2008.08.028.

[48] L.G. Homshaw, High resolution heat flow DSC: application to study of phase transitions, and pore size distribution in saturated porous materials, J. Therm. Anal. Calorim. 19 (2005) 215–234, https://doi.org/10.1007/bf01915798.

[49] J. Chang, Y. Zhang, X. Shang, J. Zhao, X. Yu, Effects of amorphous AH3 phase on mechanical properties and hydration process of C4A3S¯-CS¯H2-CH-H2O system, Construct. Build. Mater. 133 (2017) 314–322, https://doi.org/10.1016/j.conbuildmat.2016.11.111.

[50] M. Li, M. Lan, Z. Chen, J. Wang, S. Cui, Y. Wang, Research on the hydration properties of C4A3S-CSH2 cement system at different temperatures, Materials 13 (2020) 4000, https://doi.org/10.3390/ma13184000.

[51] L. Liu, G. Ye, E. Schlangen, H. Chen, Z. Qian, W. Sun, K. van Breugel, Modeling of the internal damage of saturated cement paste due to ice crystallization pressure during freezing, Cement Concr. Compos. 33 (2011) 562–571, https://doi.org/10.1016/j.cemconcomp.2011.03.001.

[52] R.E. Beddoe, M.J. Setzer, A low-temperature DSC investigation of hardened cement paste subjected to chloride action, Cement Concr. Res. 18 (1988) 249–256, https://doi.org/10.1016/0008-8846(88)90009-9.

[53] E. Kamada, Frost Damage of Concrete Considering Freezing Point Depression of Capillary Water in Hardened Cement Paste, 1988. https://eprints.lib.hokudai.ac.jp/dspace/bitstream/2115/42180/1/145_53-62.pdf.

[54] T.C. Powers, Freezing effects in concrete, Spec. Publ. 47 (1975) 1–12, https://doi.org/10.14359/17603.

[55] G. Fagerlund, Determination of pore-size distribution from freezing-point depression, Mater. Construcción 6 (1973) 215–225, https://doi.org/10.1007/BF02479036.

[56] ACI Committee, Guide to Cold Weather Concreting "ACI 306R-10,", Am. Concr. Inst. Farmington Hills Mich, USA, 2010.

[57] R. Trauchessec, J.-M. Mechling, A. Lecomte, A. Roux, B. Le Rolland, Hydration of ordinary Portland cement and calcium sulfoaluminate cement blends, Cement Concr. Compos. 56 (2015) 106–114.
[58] D. Damidot, A. Rettel, Study of the Interaction between the Hydration of CA and of C3S at Room Temperature, 2003.
[59] M. Ben Haha, F. Winnefeld, A. Pisch, Advances in understanding ye'elimite-rich cements, Cement Concr. Res. 123 (2019), 105778, https://doi.org/10.1016/j.cemconres.2019.105778.
[60] F. Winnefeld, B. Lothenbach, Hydration of calcium sulfoaluminate cements — experimental findings and thermodynamic modelling, Cement Concr. Res. 40 (2010) 1239–1247, https://doi.org/10.1016/j.cemconres.2009.08.014.
[61] Finnish Meteorological Institute, (n.d.). https://en.ilmatieteenlaitos.fi/(accessed January 2, 2022).